# Sensitivity of Coastal Currents Near Pt. Conception to Forcing by Three Different Winds: ECMWF, COAMPS and Blended SSM/I-ECMWF-Buoy Winds

Changming Dong and Lie-Yauw Oey*

Program in Atmospheric & Oceanic Sciences, Sayre Hall,
Princeton University, Princeton, NJ 08544

Submitted: January, 2004

*Corresponding Author: lyo@princeton.edu

## Abstract

Previous observational and modeling studies have indicated the importance of fine-scale winds in determining the circulation near Pt. Conception, in the Santa Maria Basin (SMB) and the Santa Barbara Channel (SBC), California. There has not been a systematic attempt, however, to analyze and quantify the sensitivity of the near-surface circulation to different wind data. Here we drive a regional circulation model (based on the Princeton Ocean Model) of the SMB and SBC using three wind data sets: the European Center for Medium-Range Weather Forecast (ECMWF; $\approx$ *110km´110km* horizontal grid), the Coupled Ocean/Atmosphere Mesoscale Prediction System (COAMPS; *9km´9km* horizontal grid) and a blended wind product, SEB, that combines SSM/I (Special Sensor Microwave/Imager), ECMWF and Buoy and coastal wind data. A spring-time period is chosen for the study (March-May 1999) when equatorward wind dominates and wind stress curls are strong. Two groups of experiments are conducted: with and without assimilating moored temperature observations. Comparisons between these experiments and between model and observation show that the circulation driven by the ECMWF wind is much weaker than that by the other two winds. On the other hand, the SEB dataset shows locally intensified wind stress curls behind Capes and coastal bends, while these wind stress curls are weak or non-existence in COAMPS. It is found that these small-scale variations in the wind field force along-shore inhomogeneous pressure gradients that in turn can significantly impact the near-coast currents. The result is that modeled currents forced by SEB agree better with observations than those produced by COAMPS. Empirical orthogonal analyses (EOF) were conducted on the near-surface currents, sea-level, wind and wind stress curl. The mode-1 current ($\approx$ *40%*)

is unidirectional (i.e. generally equatorward or poleward) and correlates well with the mode-1 wind ($\approx$ *90%*). The mode-2 current ($\approx$ *20%*) is cyclonic in the SBC and poleward-inshore and equatorward-offshore in the SMB; it correlates well with mode-1 sea-level ($\approx$ *70%*), which suggests that mode-2 currents are driven by the pressure-gradient. Significantly, neither mode-2 current nor mode-1 sea-level correlates well with mode-1 wind stress curl ($\approx$ *70%*); rather, they correlate well with the time-integral of the mode-1 wind-stress curl. These conclusions support a previous theoretical idea that cyclonic circulation in the SBC and the inshore currents of the SMB are both driven by alongshore pressure set-up induced by the time-integral of the wind stress curl, rather than by the wind stress curl itself. This idea of a pressure set-up is consistent with the differences found above between the currents driven by COAMPS and SEB winds.

## 1. Introduction

The importance of wind stress and wind curl to the near-surface circulation near Pt Conception, the Santa Barbara Channel (SBC) and Santa Maria Basin (SMB), California (see Fig. 1), is now well documented (Oey, 1996, 1999; Wang, 1997; Harms and Winant, 1998). Harms and Winant (1998) showed that surface currents depend on the wind stress and (along-shore) pressure gradients in the SBC. The along-shore gradient of wind curl may build up a pressure gradient against the wind direction, and can force a poleward current nearshore when the wind relaxes (Oey, 1996,1999; Wang, 1997). Winant et al (2003) further studied the seasonal variation of the circulation and categorized it into three patterns: upwelling (spring), convergence (summer), and relaxation (fall and winter). These studies suggest that near-surface currents in SBC and SMB are sensitive to wind.

The seasonal variation of wind in the SMB and SBC is described in detail by Dorman and Winant (2000). In spring and summer, winds become persistently equatorward and intensified west of the SBC but diminish toward the east. Based on the California Cooperative Fishery Investigation (CalCOFI) ship wind data, Winant and Dorman (1997) divided the wind stress in spring and summer into two regions: a high-wind zone in the area offshore from a line between Point Conception and Ensenada, Mexico, and a low-wind zone inshore of the line. They showed the sharp local change in the wind stress and wind stress curl: high-wind zone extends throughout the entire offshore region west and south of the SBC and the maximum wind stress and maximum wind stress curl are located off Point Conception. The wind variation scale is about 10-30

km. To incorporate the sharp change in wind stress and wind stress curl, a high-resolution wind is needed for the simulation of the circulation in this region.

In a previous numerical simulation of the circulation in SBC and SMB (Oey et al, 2003), the wind used to drive the ocean is a combination of the European Center for the Medium Range Weather Forecast (ECMWF) wind (which has a coarse resolution of about 1.125°) and local meteorological stations by Optimum Interpolation (OI). Oey et al.'s work shows that the circulation forced by the wind captures the cyclonic circulation in the western part of the SBC and its seasonal variation. By incorporating wind data from coastal stations with ECMWF wind, Oey et al (2003) show that the modeled circulation is in better agreement with observations than that forced by the coarse-grid ECMWF wind only. In this paper, we extend Oey et al.'s work and examine more closely the sensitivity of the ocean currents to forcing by different wind datasets. Apart from the ECMWF, two higher-resolution wind datasets are used in this work.

Dong et al (2003) produced a new wind data set in SMB and SBC by combining three wind data sets: the SSM/I (Special Sensor Microwave/Imager) wind data from satellite remote sensing, ECMWF wind, and wind data from thirty-two buoy and other coastal wind stations (marked as circles in Fig. 1) deployed by the National Data Buoy Center (NDBC) and the Minerals Management Service (MMS). Dong et al. (2003) found that the ECMWF wind agreed well with offshore (≈ 50 km and more from the coast) buoy wind data. However, the ECMWF speeds are weaker than buoy data especially near the coast. The ECMWF wind directions were therefore retained while its speeds were replaced by SSM/I speeds after the latter have been cleaned and edited for errors. An OI scheme was then used to merge this ECMWF-SSM/I composite dataset with wind

data from NDBC buoys and other coastal meteorological stations. The blended wind is hereinafter referred to as the SEB (for SSM/I, ECMWF and Buoy) wind; it is six-hourly on a 5km×5km grid covering the rectangular ocean model domain shown in Figure 1a.

Hsu et al (2003) used the Navy's nested-grid regional model: the Coupled Ocean/Atmosphere Mesoscale Prediction System (COAMPS) to produce wind for the period 03/01/99-05/31/99. The inner-most nest includes the SMB and SBC and has a horizontal resolution of 9km×9km. The simulated winds were found to agree well with buoy observations especially offshore in the western portion of the SBC and SMB. The results deteriorate in the eastern SBC and very near the coast (~10 km). The authors suggest that the 9km-resolution is still insufficient to resolve sharp changes in coastal topography and to simulate hydraulic jumps that often occur in the eastern SBC (Dorman and Winant, 2000). The COAMPS wind is also sampled six-hourly and interpolated on to the same 5km×5km SEB (or ocean model) grid.

In the present study, we examine the responses of the near-surface circulation to the SEB, COAMPS and ECMWF winds during the period March 1 through May 31, 1999. We wish to study the sensitivity of the near-surface currents to the wind stress and its small scale features in the SMB and SBC. During the study period, the region is characterized by a transition to more persistent upwelling-favorable wind in the SMB and a strong wind stress curl in the SBC. Since wind stress curls reveal smaller-scale variations in the wind field, it is necessary that higher resolution and high quality winds (as outlined above) are used in the ocean modeling and also in analysis.

The paper is organized as follows. In Section 2, the SEB, COAMPS and ECMWF winds are compared. In Section 3, the model configuration and numerical experiments

are described. In Section 4, numerical experiments are compared with each other and with observations. In Section 5, Empirical Orthogonal Function (EOF) analysis is presented. Section 6 is discussion and summary.

**2. Wind Data**

Figure 2 shows the three-month averaged (March-May, 1999) wind stress (a) and wind stress curl (b) for the three wind datasets: ECMWF, COAMPS and SEB. (In this and the following maps, a more detailed sub-region of the model domain encompassing the SMB and SBC are shown). The general directions of the three winds are similar. The ECMWF wind is much weaker than COAMPS and SEB winds, especially near the shore. This may be attributed to the coarse resolution used in the ECMWF wind. Small-scale variations are smoothed out in the ECMWF wind, and the corresponding wind stress curls are also weaker than the other two winds. The strengths and directions of COAMPS and SEB winds are similar. Both show strong equatorward winds over the SMB and west of SBC, and rather rapid weakening eastward into the SBC. The SEB wind shows localized strong speeds approximately 30 km offshore in the SMB and also in the western SBC. No such localized strong speeds exist in the COAMPS wind. Instead, the COAMPS wind is more uniform alongshore. Differences can be seen clearly in the corresponding wind stress curls (Figure 2b). The ECMWF wind stress curl is weak, less than 0.1 Pa/100 km throughout the region. COAMPS gives strong wind stress curl near the shore, and cells of localized maxima along the coast with values that reach 0.3~0.4 Pa/100 km. The SEB wind stress curl near the shore is also strong, but there are two well-organized localized maxima: one downwind of Pt. Buchon (values ≈ 0.3~0.4

Pa/100km) and another one downwind of Point Conception (values ≈ 0.5 Pa/100km). The SEB wind also shows an alongshore band of negative curl (albeit weak) at approximately 50km offshore. These SEB wind features (localized maximum wind stress curls behind Capes and band of negative curl offshore) are known in observations (Dorman, 2003; personal communication). We now show that these subtle differences in wind and wind stress curl have important consequences to the near-shore circulation.

## 3. Model Configuration and Experiments

### *a. Model Configuration*

The model is based on the Princeton Oceanic Model (Mellor, 2002), and its configuration is similar to that used by Oey et al (2001,2003) in their study of the dynamics of cyclonic circulation and upwelling in the Santa Barbara Channel. Here we briefly describe it. The model grid extends 300 km offshore and 550 km in the alongshore direction (Figure 1a). The horizontal grid resolution is constant, ?x=?y=5 km. The grid is rectangular and axes have been rotated 52° anti-clockwise. The vertical grid consists of 30 equally spaced sigma-levels. The western boundary condition consists of a radiation condition with a sponge layer, within which the horizontal viscosity is linearly increased 10 times its interior value within 10 grids. The sponge layer damps westward propagating Rossby waves and helps to prevent the development of an artificial boundary layer. The northern and southern boundary conditions are also radiation with sponge layers. Normal fluxes are zero cross all closed boundaries. Across open boundaries, temperature and salinity are advected during outflow and specified using monthly

climatological data at inflow. Climotological temperature and salinity are also used for initial condition (Levitus, 1982, 1994).

*b. Numerical Experiments*

As part of a more extensive modeling study to be reported elsewhere (Dong and Oey, 2003; work in progress), the SEB wind was used to force the model ocean from a rest state starting on January 1, 1992, and integrated through 1999. For the present study, the initial condition is the model ocean state at the end of February, 1999. A series of numerical experiments are performed with the three winds. Each integration is for three months, March through May 1999. These experiments are divided into two groups: without and with temperature assimilation. As in Oey et al (2003), the temperature assimilation uses the statistical interpolation method (Daley, 1990; Chen and Wang, 1999,2000). Temperatures at twelve mooring stations are used in the assimilation; these are marked by the square symbols in Figure 1a and 1b. Details of the observations are given by Harms and Winant (1998) and Winant et al. (2003). The experiments are summarized in Table 1.

**4. Experiment Results**

*a. Wind-Only Experiments 1, 2 and 3*

The mean near-surface currents (at z = −5m) and sea surface height (SSH) for the wind-only experiments are shown in Figures 3a and 3b, respectively. Here and in subsequent analyses, the mean (or analysis period) is taken as the average over the period

from March 10 to May 31, thus excluding a 10-day (March 1-10) initial adjustment of the model dynamics to wind. Superimposed on the model current maps are also mean observed currents (heavy vectors; also at z = −5m) for the same period. The figures show two primary circulation features: a southward flow in the SMB and cyclonic circulation in the western part of the SBC. The near-shore upwelling in the SMB and the upwelling in the cyclonic circulation in the western SBC show up as low's in the SSH contours in Figure 3b. It is clear that currents driven by the ECMWF wind (Exp.1) are weaker than those driven by the COAMPS wind (Exp.2) or the SEB wind (Exp.3). As discussed previously, the ECMWF wind is the weakest among the three winds and its resolution near the coast is not sufficient to resolve small-scale wind structures (Figure 2). In Exp.3, there are two localized upwelling centers: one off Point Buchon and the other, stronger one off Point Conception. These correspond to the two local maxima in the wind stress curl seen in Figure 2b. By contrast, Exp.1 and Exp.2 show only one upwelling center in the SBC. In Exp. 1, the upwelling is weak. In Exp. 2, the upwelling is strong and extends further east into the channel. In the SMB, the mean near-surface currents driven by both ECMWF (Exp. 1) and COAMPS (Exp. 2) veer offshore near 35° N, while currents driven by the SEB wind (Exp. 3) are more intense and more aligned with the coast. This along-shore alignment of the currents (for Exp.3) in the SMB agrees better with the observed currents (Figure 3a).

The above differences in the circulation pattern can be understood by examining the momentum balance. Figure 4 shows the mean momentum balance in both the along-shore and cross-shore directions at the section SAIN in the SMB (marked as a solid line in Figures 1 and 3) for the three experiments. The balance is primarily among the wind

stress (dash; strictly speaking it is the vertical divergence of vertical shear stress; near the surface the term is dominated by the wind stress; c.f. Oey et al. 2003), pressure gradient (dash-dot) and Coriolis term(solid). Tendency and advection are small. The cross-shore balance for the three experiments are similar near the coast: the offshore Coriolis force (due to equatorward along-shore current) is balanced by the onshore wind stress and pressure gradient. In Exp.3, the balance is primarily geostrophic, $fv \approx (\partial p/\partial x)/\rho_o$ especially within about 40km of the coast, while in exp.1 and exp.2 $(\partial p/\partial x)/\rho_o$ is weaker and the wind stress term becomes relatively more important. In the along-shore direction, momentum balances for the three experiments are different. The wind stress term is equatorward for all three experiments. The Coriolis term is directed poleward in Exp.1 and Exp.2 but in Exp.3 it changes sign from poleward offshore to become equatorward within 40km of the coast. The pressure gradient is equatorward in Exp.1 and Exp.2 but poleward and rather large in Exp.3. Figure 3b indicates that the poleward pressure gradient in Exp.3 is caused by the low (upwelling) center just south of Point Buchon. This pressure gradient overcomes equatorward wind stress in producing onshore flow with equatorward Coriolis component. The onshore convergence helps to maintain the equatorward jet south of 35° N, as seen in Figure 3a for Exp. 3. In contrast, no localized upwelling center south of Point Buchon exists for Exp.1 or Exp.2. The corresponding pressure gradient is equatorward, which together with the equatorward wind stress produces offshore flow. As a result, the coastal jets in Exp.1 and Exp.2 are less well-defined as the currents tend to veer offshore south of 35°N (Figure 3a). Considering that the along-shore pressure gradient in part comes from the wind curl and

its spatial variation (Oey, 1999), the above differences clearly show the subtle sensitivity of coastal currents to wind and wind stress curl along the coast.

*b. With Temperature Assimilation: Experiments 1a, 2a and 3a*

For experiments with temperature assimilation, the three-month averaged near-surface currents and SSH are plotted in Figures 5a and 5b, respectively. Compared with the results without assimilation (Figure 3), the near-surface currents in the SMB for Exp.1a and Exp.2a now become more intensely equatorward, and more aligned with the coast, in better agreement with the observed currents and also with Exp.3. The adjustment in Exp.3a is less, but currents near the coast improve (become somewhat stronger). We conclude that data assimilation "corrects" deficiency in model physics and forcing (wind; in Exp.1 and Exp.2 in particular) and adjusts the modeled currents towards observations. The 'correction' can be seen in the SSH plot in figure 5b. Comparing with figure 3b, we see that assimilation alters the pressure field such that Exp.1 and Exp.2 now show SSH low's downwind of Point Buchon (the corresponding low for Exp.3 is also strengthened), and the SSH low in the western SBC for Exp.1 is strengthened. As the momentum-balance analysis (Figure 4) shows, the existence of a Point Buchon low is crucial in forcing onshore convergence and stronger coastal jet in the SMB. That the 'correction' is minor in Exp.3a suggests that the SEB wind may be a more appropriate data set than the coarse-resolution ECMWF or the 9 km-resolution COAMPS winds. Note that the three wind vectors are quite similar, especially COAMPS and SEB. All show equatorward wind (Figure 2a). The differences are subtle, especially in their curls near the coast (Figure 2b).

In the SBC, the cyclonic cell is enhanced for all three wind experiments with data assimilation. The effects of data assimilation are not as large as those in the SMB, however, as there are only three stations available for assimilation (Figure 1b).

c. *Model-Observation Comparisons*

Some comparisons of the modeled and observed currents at z = −5m have been presented above (figures 3 and 5). In the SMB, observed currents show strong along-shore jet (speeds ≈ 0.2 m $s^{-1}$). All experiments underestimate the jet especially at stations inshore, although as mentioned previously Exp.3 gives the best overall agreement in that the modeled jet aligns along-shore as are also observed. Assimilation improves the agreements though the modeled currents inshore are still weak. The reason may be that model resolution can become more of an issue for near-shore currents. (The first-mode baroclinic Rossby radius of deformation estimated from climatology is ≈ 5 km comparable to model grid size, though one clearly needs a fraction of this to resolve fine-scale flow structures; Oey, 1998). In the SBC, only three moorings are available for comparison. Observed currents at the two western stations (SMIN and SMOF) are oppositely directed indicative of a cyclonic recirculation (Harms and Winant, 1998). All experiments also indicate this western cyclone, though Exp.1 with ECMWF is the weakest. Assimilation improves the strength of the cyclone (c.f. Oey et al. 2003). At the lone eastern mooring (ANMI), the observed mean is weak. Both Exp.1 and Exp.3 show also weak means (Figure 3) but for different reasons; the former is because currents in Exp.1 are everywhere generally weak (due to weak ECMWF near-coast), while the latter is because the strong SEB wind stress curl is confined to the western SBC (Figure 2b).

By contrast, the COAMPS wind stress curl in Exp.2 extends further into the channel, and modifies the pressure field (Figure 3b) that allows a stronger poleward flow into the channel (Figure 3a). Assimilation has relatively minor effects on modeled currents at ANMI (Figure 5a).

Figure 6 compares current variance ellipses for all experiments. The model generally underestimates variances. Experiment 1 gives the lowest variances while Exp.3 gives better overall agreements with observations especially in the SMB. There are some improvements for experiments with assimilation (Figure 6b). Observed currents at ANMI show large fluctuations, which are missing from all the model experiments. As in Oey et al. (2003) effects of remote forcing (from the south) are not well simulated in the model but are potentially important at ANMI (Auad and Hendershott, 1997; Hickey et al., 2003).

**5. EOF Analysis**

We further analyze effects of different wind forcing by examining the empirical orthogonal functions (EOF) of currents, wind and wind stress curl. In the EOF analysis, the grid points used are further confined to the SMB and SBC. The first modes of wind stresses for ECMWF, COAMPS and SEB are generally directed along-coast (along-channel), and explain over 85% of their variances (Figure 7). Their time series are quite similar in phase, but the weather cycles (time scales of about 5~10 days) in COAMPS and SEB are more energetic. The first modes of the wind stress curls explain over 70% of their variances (Figure 8). The along-shore patterns are similar to the corresponding wind stress curl maps of figure 2b: little variation for ECMWF and cellular structures for

COAMPS and SEB. The two organized 'cyclonic' structures with maximum EOF's downwind of Pt. Buchon and Pt. Conception are clearly seen in the SEB map. Note that, as will be explained below, the time-integrated time series of the wind stress curl rather than its time series are shown in Figure 8.

The EOF analysis of the near-surface currents shows that the first and second modes explain nearly over 60% of the variance (Figure 9). The first mode (figure 9a, left panels) is "unidirectional" and in the SBC resembles the wind-forced upwelling pattern described in Oey et al. (2001). This mode explains nearly 40% of the total variances. The corresponding time series closely resembles the first mode of wind stress (c.f. figure 7); the correlation coefficients exceed 0.90 for all three experiments (1, 2 and 3; figure 9b). The high correlation confirms that the first mode of current is primarily driven by along-coast (along-channel) wind.

The second mode of the near-surface current shows oppositely directed along-coast flow patterns across the SBC or across the SMB shelf/slope, i.e. "cyclonic" structure. This mode accounts for over 18% of the variances (Figure 9a, right panels). The corresponding time series (figure 9b, right panels) changes sign near mid-April. Thus the inshore flow for this mode changes from equatorward to poleward. The change is small or almost non-existence for Exp.1, but significant for Exp.2 and Exp.3. The sign-change indicates the strengthening of the western SBC cyclone from early to late spring (Oey et al. 2003). One might speculate that the strengthening is directly related to wind stress curl (c.f. Munchow, 2000). However, the correlation between the first mode wind stress curl and the second mode of surface current is very poor, less than 0.1. On the other hand, Oey's (1996; 1999) analysis shows that the presence of inhomogeneous

alongshore wind stress curl can induce near-shore currents, and that the relevant forcing function is the time-integral of the wind stress curl gradient along the coast, rather than the wind stress curl itself. In the present case, a proxy of this function is simply the time-integral of the mode-1 EOF of the wind stress curl. This time-integral function is plotted in figure 8 (right panels). For Exp.1, the correlation between this function and mode-2 current is weak, ≈ 0.4. For Exp.2 and Exp.3, the correlation is high, ≈ 0.74 (figure 9b). The high correlation suggests that the fluctuating near-shore flow (hence also the cyclone) is in part driven by the time-integral of the wind stress curl.

The existence of poleward inshore flow in the upwelling zone has long been recognized. McCreary et al (1987) proposed two possible mechanisms: the one is induced by the positive wind curl, and the other by the relaxation of the upwelling-favorable wind stress. Oey (1996, 1999) suggests that the poleward near-shore current is driven by the poleward pressure gradient, and the gradient is proportional to along-shore gradient of the time-integrated wind stress curl. Wang (1997) showed how a strong poleward alongshore pressure gradient is produced by a positive wind stress curl and drives an inshore poleward current into the upwelling zone. Münchow (2000) found a significant correlation between the wind stress (which is proxy for wind stress curl) and the cyclonic shear observed at the western entrance to the channel using the observation data from January to July of 1984. Dever (2003) showed that the velocity potential indicates a source term in the western SBC consistent with the wind stress curl-driven circulation. Here the high correlation between the mode-2 EOF of currents and the time-integrated mode-1 EOF of the wind stress curl further confirms the relationship between the wind

stress curl and the poleward inshore flow. We have confirmed here that the relationship is between the *time-cumulated* positive wind stress curl and the fluctuating inshore flow.

To further explain how the external force (wind stress curl) drive the inshore poleward flow in the coastal region, we calculate the EOF's of SSH (figure 10). The first mode accounts for over 60% of the total variance and its spatial pattern clearly shows the along-shore pressure gradient. The correlation coefficients between the mode-1 SSH and the mode-1 time-integrated wind stress curl is 0.58 for Exp.1, and 0.78 for both Exp.2 and Exp.3. The correlation coefficients between mode-1 SSH and mode-2 current are 0.77, 0.87 and 0.75 for Exp.1-3, respectively. These high correlations reveal that the poleward flow is driven by poleward pressure gradient, and the pressure gradient is set up by the time-integrated wind stress curl. The conclusion agrees with Oey's (1996, 1999) and Wang's (1997) analyses.

**6. Summary**

This paper examines the sensitivity of modeled currents in the SBC and SMB to forcing by three different wind datasets: the ECMWF reanalysis wind, the Navy's regional model COAMPS wind, and SEB, a wind product that we have derived using satellite SSM/I, ECMWF and coastal buoy data. The ECMWF wind has coarse resolution (≈ 110 km) and is not suitable for circulation modeling in coastal region that has significant wind stress and wind stress curl. The resulting modeled currents are weak and are quite different from observations. Both COAMPS and SEB winds generally produce more energetic currents. In particular, the cyclonic circulation in the western SBC is reproduced well. Subtle differences exist, however, between the two winds,

especially in the corresponding wind stress curls. Well-organized local maxima in wind stress curls exist behind Capes in the SEB dataset, while COAMPS show a series of cellular wind stress curl patterns along the coast. Alterations to the flow momentum balance are significant. The upshot is a model current field forced by SEB that agrees better with observations. EOF analyses show the dominance of two current modes: a mode-1 with 'unidirectional' spatial structure that is forced by the wind, and a mode-2 'cyclonic' spatial structure with poleward inshore flow that is forced by the time-integral of the wind stress curl. This latter finding confirms Oey's (1996, 1999) and Wang's (1997) analyses.

**Acknowledgements**

We thank Ed Dever for providing the observational data. This work was funded by the Minerals Management Service and the Office of Naval Research. Computing was done at GFDL, NOAA.

**References:**

Auad, G. and M.C. Hendershott, 1997: The low-frequency transport in the Santa Barbara Channel: description and forcing. *Continental Shelf Research* (17)7, 779-802.

Chen, C.-S. and D.-P. Wang, 1999: Data assimilation model study of the Santa Barbara Channel, *JGR-Oceans*, 104, 15,727-15,472.

Chen, C.-S. and D.-P. Wang, 2000: Data assimilation model study of wind effects in the Santa Barbara Channel, *JGR-Oceans*, 105, 22,003-22,013.

Daley, 1990,

Davis, R.E., 1976: Predictability of sea surface temperature and sea level pressure anomalies over the North Pacific Ocean, *J. Phys. Oceanogr., 3,* 249-266.

Dever, E.P., M.C. Hendershott and C.D. Winant, 1998: Statistical aspects of surface drifter observations of circulation in the Santa Barbara Channel. *JGR-Oceans*, 103, 24,781-24,797.

Dever, E.P. 2003: Objective Maps of Near-Surface Flow States near Pt. Conception, California, submitted to *J. Phys. Oceanogr.*.

Dong, C.M., L-Y Oey and H. Zhang, 2003: Synthetic Winds for the Central and Southern California Coastal Ocean, Princeton University AOS Program Report, 2003-01-02.

Dorman, C.E. and C.D. Winant, 2000: The structure and variability of the marine atmosphere around the Santa Barbara Channel. *Mon. Wea. Rev.*, 128, 261-282.

Harms, S. and Winant, C.D. 1998: Characteristic patterns of the circulation in the Santa Barbara Channel. *JGR-Oceans*, 103: 3041-3065.

Hickey, B.M., 1979: The California Current System: Hypotheses and facts, *Prog. Oceanogr.*, 8, 191-279.

Hickey, B.M., 1992: Circulation over the Santa Monica-San Pedro basin and shelf. *Prog. Oceanogr.*, 30, 37-115.

Hickey, B.M., E.L. Dobbins, and S.E. Allen, 2003: Local and remote forcing of currents and temperature in the central Southern California Bight. *J. Geophys. Res.*, 108 (C3), 3081, doi:10.1029/2000JC000313.

Hsu, H-M, L-Y Oey, C. Dong, C. Dorman and R. Hodur, 2003: A Regional Atmospheric Model in a Coastal Zone with Significant Wind and Wind Stress Curl: Comparison with Wind Station and Satellite Observations, to be submitted.

Large, W.G. and S. Pond, 1981: Open ocean momentum flux measurements in moderate to strong winds, *J. Phys. Oceanogr., 11,* 324-336.

Levitus, S., 1982: Climatological Atlas of the World Ocean, NOAA Professional Paper 13, 174 pp., U.S. Government Printing Office, Washington, D.C.

Levitus, S., 1994: World Ocean Atlas 1994 CD-Rom sets. National Oceanographic Data Center Informal Report, 13.

McCreary, J.P., P.K. Kundu and S.Y Chao, 1987: On the dynamics of the California Current System. *J. Mar. Res*. 45(1), 1-32.

Mellor,G.L., 2002. User's Guide: http://www.aos.princeton.edu/WWWPUBLIC/htdocs.pom.

Munchow, A. 2000: Wind stress curl forcing of the coastal ocean near Point Conception, California. *J. Phys. Oceanogr.*, 30, 1265-1280.

Oey, L.-Y. 1996: Flow around a coastal bend: a model of the Santa Barbara Channel eddy. *JGR-Oceans*, 101, 16,667-16,682.

Oey, L-Y. 1998. Eddy energetics in the Faroe-Shetland Channel, *Cont. Shelf Res.*, 17: 1929-1944.

Oey, L.-Y. 1999. A Forcing Mechanism for the Poleward Flow off the Southern California Coast, *JGR-Oceans*, 104, 13,529-13,539.

Oey, L.-Y., D.-P. Wang, T. Hayward, C. Winant, & M. Hendershott. 2001: Upwelling and cyclonic regimes of the near-surface circulation in the Santa Barbara Channel. *JGR-Oceans*, 106, 9213-9222.

Oey, L.-Y., C. Winant, E. Dever, W. Johnson, and D.-P. Wang, 2003: A data-assimilated model of the near-surface circulation of the Santa Barbara Channel. *JPO*, in press. (Available through http://www.aos.princeton.edu/WWWPUBLIC/PROFS/ under "Publications.").

Wang, D.-P., 1997: Effects of small-scale wind on coastal upwelling with application to Point Conception. *JGR-Oceans*, 102, 15,555-15,566.

Winant, C.D. and C.E. Dorman. 1997: Seasonal patterns of surface wind stress and heat flux over the Southern California Bight. *JGR-Oceans*, 102, 5,641-5,653.

Winant, C.D., E.P. Dever and M.C. Hendershott, 2003: Characteristic patterns of shelf circulation at the boundary between central and southern California J. Geophys. Res. (Ocean), Vol. 108 No. C2, 10.1029/2001JC001302.

**Table and Figure Captions**

**Table 1** A summary of the numerical experiments

**Fig. 1** a) A locator map of the ocean region of interest. The rectangle is the ocean model domain. Light contours denote the 200m, 500m and 2000m isobaths. Circles denote the 32 meteorological stations (for wind data) and squares denote the 12 mooring stations for temperature and current data. b) The locations and names of the twelve mooring stations.

**Fig. 2** a) The three-month mean wind stress vectors obtained from ECMWF (left), COAMPS (middle), and SEB (right). Contours indicate wind stress magnitudes and the contour interval is 0.2 $dyn/cm^2$. b) The three-month mean contours of the wind stress curl for ECMWF (left), COAMPS (middle), and SEB (right). The contour interval is 0.2 Pa/100km.

**Fig. 3** a) The three-month mean currents at z = −5m for wind-only experiments: Exp. 1 (left), Exp. 2 (middle) and Exp. 3 (right). The heavy-solid vectors are the observed mean currents (also at z = −5m) at the 12 mooring stations. The solid line is the SAIN section. b) The three-month mean sea surface elevation for wind-only experiments: Exp. 1 (left), Exp. 2 (middle) and Exp. 3 (right). The contour interval is 1cm.

**Fig. 4** Momentum balances at the cross Section SAIN (indicated in Figures 1 and 3) for Exp.1 (top), Exp.2 (middle) and Exp.3 (bottom)**.** The left panel is for cross-shore balance and the right panel is the along-shore balance.

**Fig. 5** Same as Fig. 3 except for the experiments with data (temperature) assimilation.

**Fig. 6** Comparisons of the surface current variances between model (blue) and observations (red) at 5m for a) the wind-only experiments and b) for the experiments with

data (temperature) assimilation. Left panel is ECMWF, middle is COAMPS and right is SEB. Contours are isobaths: 200m, 500m and 2000m.

**Fig. 7** EOF analysis for wind: the left panel is the spatial pattern of the first mode and the right panel is the time series of the first mode, for ECMWF (top), COAMPS (middle) and SEB winds (bottom).

**Fig. 8** EOF analysis for wind stress curl: the left panel is the spatial pattern of the first mode, and the right panel is the time-integrated time series of the first mode of the wind stress curl, for ECMWF (top), COAMPS (middle) and SEB winds (bottom).

**Fig. 9** EOF analysis for the near-surface currents for the wind-only experiments, ECMWF (top), COAMPS (middle) and SEB (bottom): a) the left panel is the spatial pattern of the first mode and the right panel the second mode; b) the left panel is the time series of the first mode and the right panel for the second mode. CC on the left panel denotes the correlation coefficient between the first mode of the surface current and the first mode of the wind stress. CC on the right panel denotes the correlation coefficient between the second mode of the surface current and the time-integrated first mode of the wind stress curl.

**Fig. 10** EOF analysis for the sea surface elevation: the left panel is the spatial pattern for the first mode and the right panel their time series for Exp. 1 (upper), Exp. 2(middle) and Exp. 3 (lower), respectively. CC1 denotes the correlation between the first mode of the surface elevation and the time-integrated first mode of wind curl, CC2 the correlation between the first mode of the surface elevation and the second mode of the surface current.

**TABLE 1**. A summary of numerical experiments

| Exps | Wind | assimilation(T) |
|---|---|---|
| 1 | ECMWF | No |
| 2 | COAMPS | No |
| 3 | SEB | No |
| 1a | ECMWF | Yes |
| 2a | COAMPS | Yes |
| 3a | SEB | Yes |

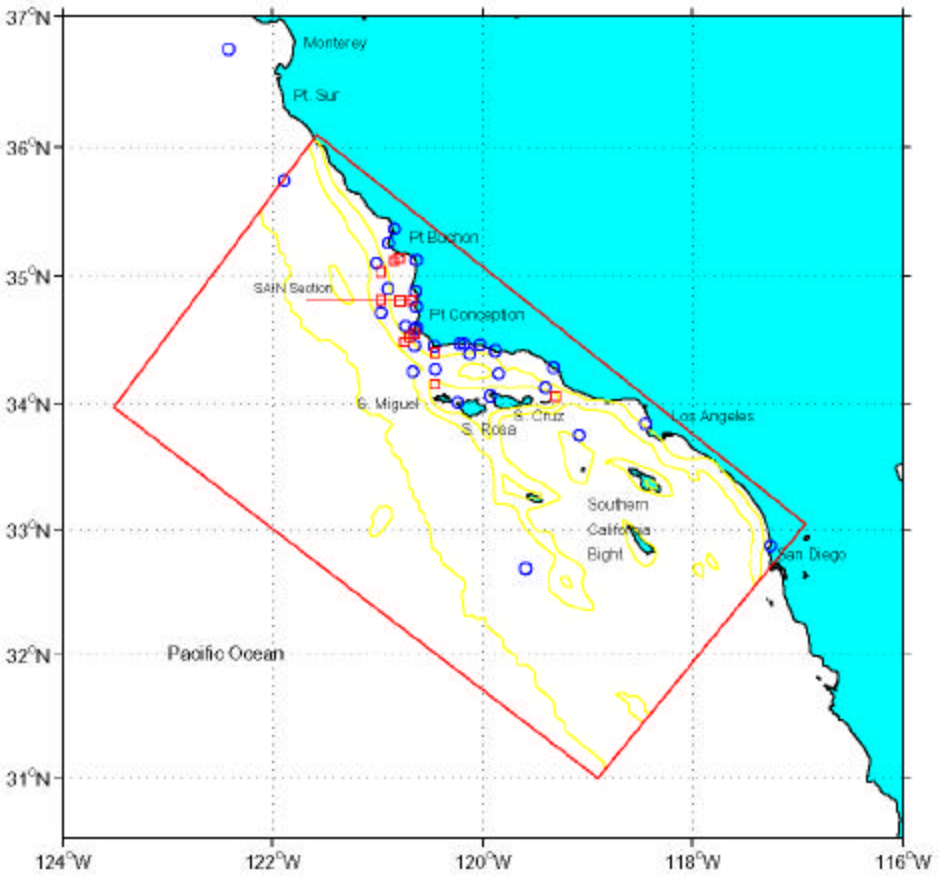
37°N
36°N
35°N
34°N
33°N
32°N
31°N
124°W
122°W
120°W
118°W
116°W
Monterey
Pt. Sur
Pt Buchon
SAIN Section
Pt Conception
S. Miguel
S. Cruz
S. Rosa
Los Angeles
Southern
California
Bight
San Diego
Pacific Ocean

Fig. 1a

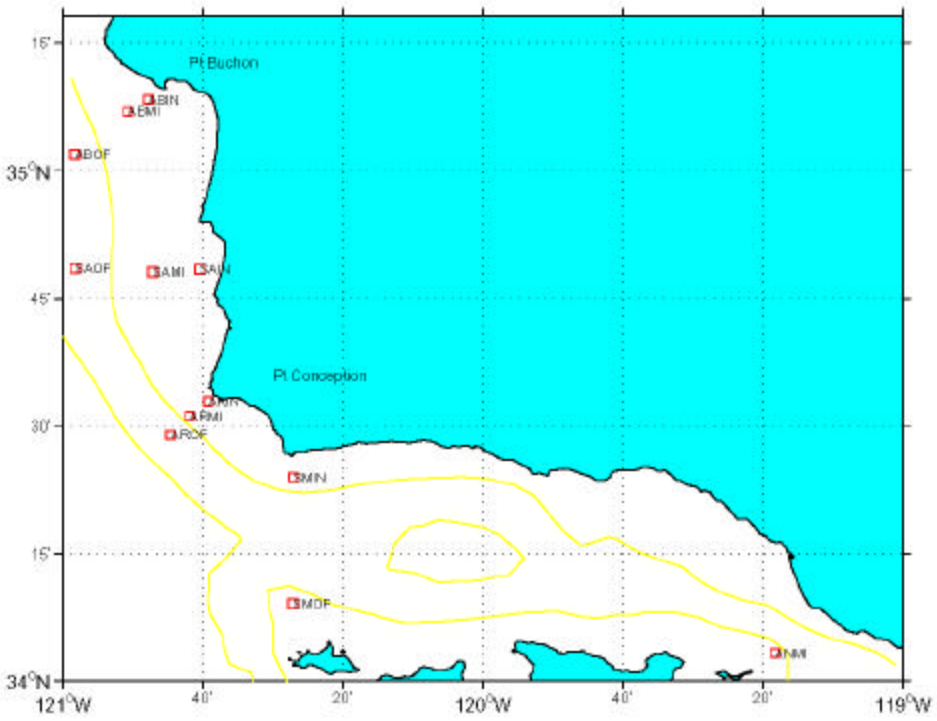
Pt Buchon
BIN
BMI
BOF
SADF
SAMI
SAIN
Pt Conception
SMIN
SPMI
SRDF
SMIN
SMDF
SNMI
35°N
34°N
121°W
120°W
119°W
15'
45'
30'
40'
20'

Fig. 1b

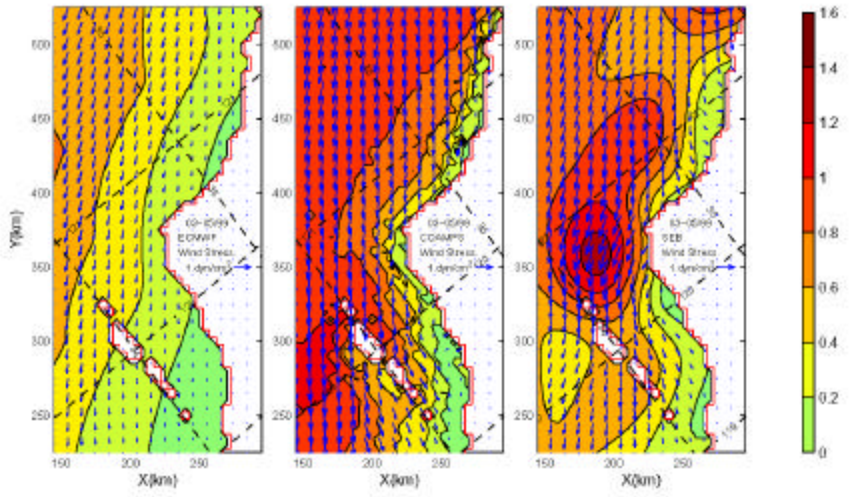


Fig. 2a

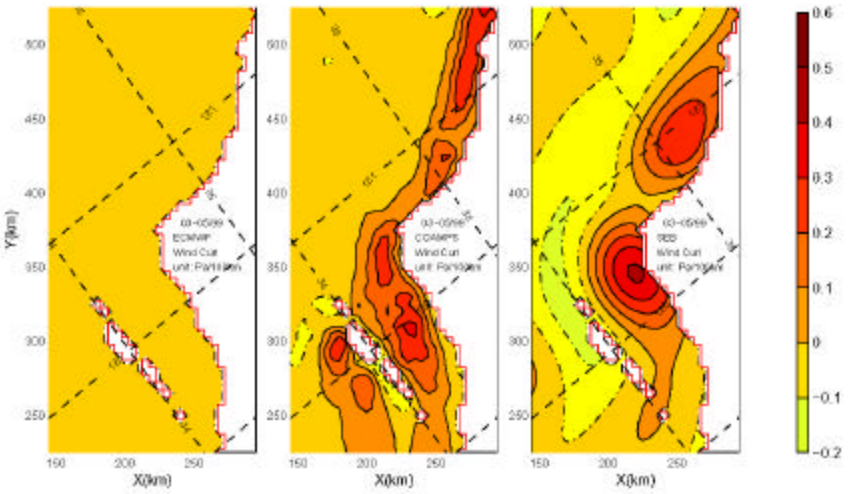


Fig. 2b

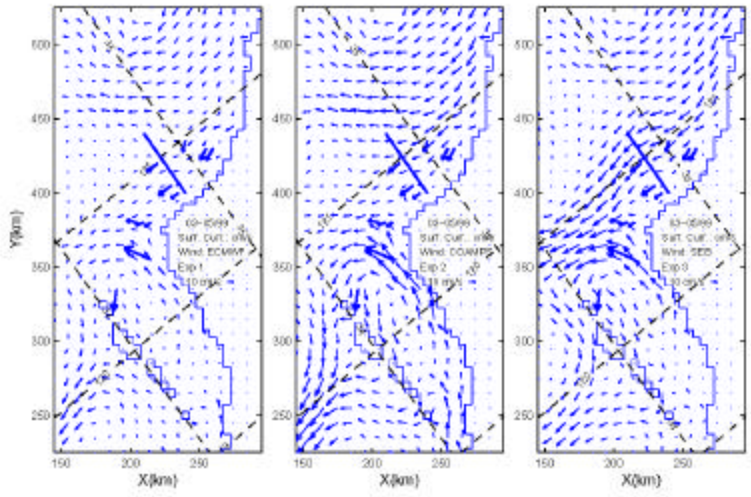


Fig. 3a

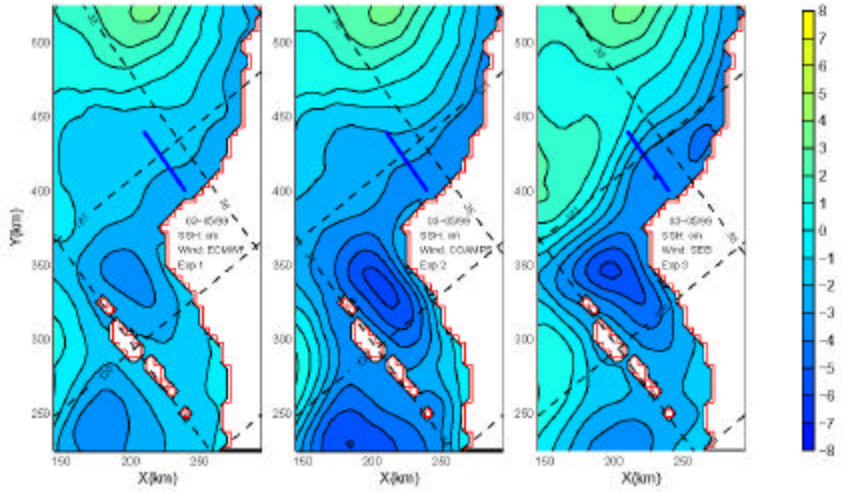


Fig. 3b

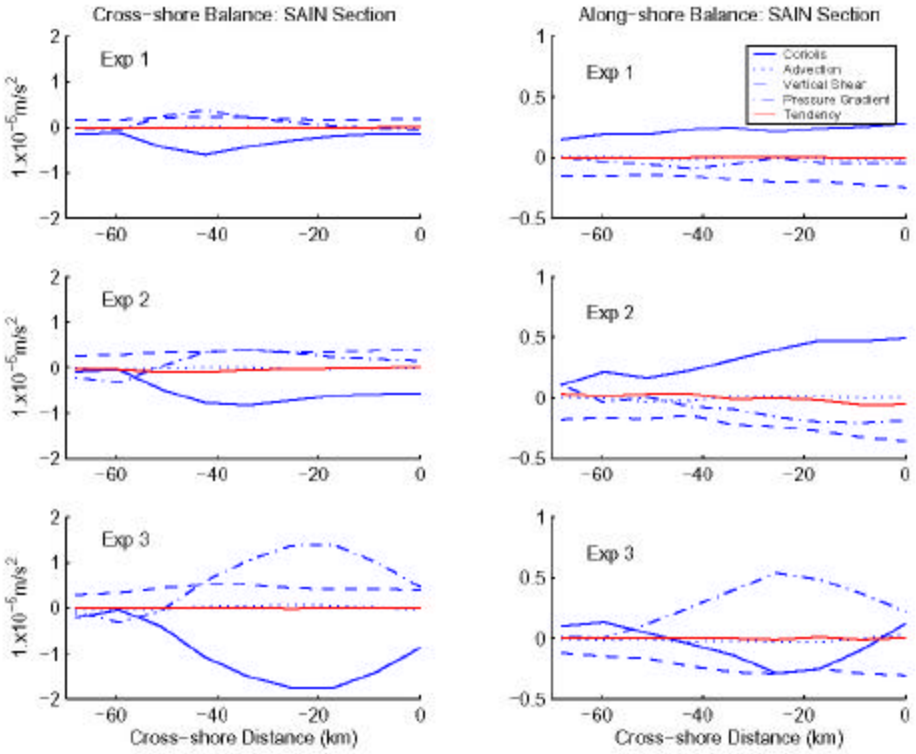
Cross-shore Balance: SAIN Section
Along-shore Balance: SAIN Section
Exp 1
Exp 2
Exp 3
Coriolis
Advection
Vertical Shear
Pressure Gradient
Tendency
1 x10^-5 m/s^2
Cross-shore Distance (km)

Fig. 4

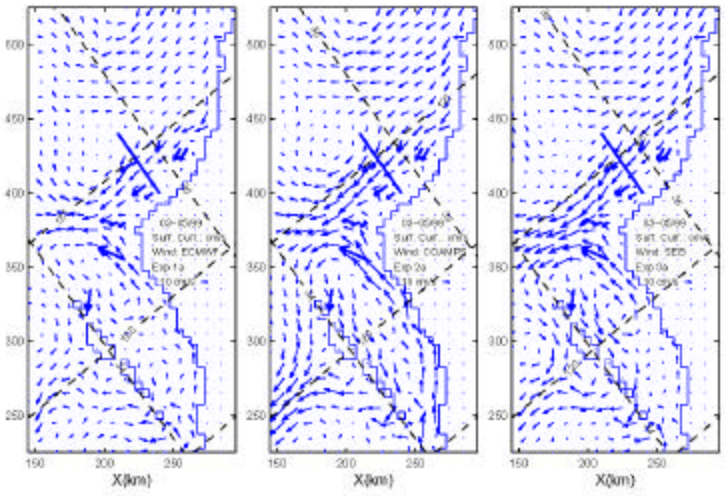


Fig. 5a

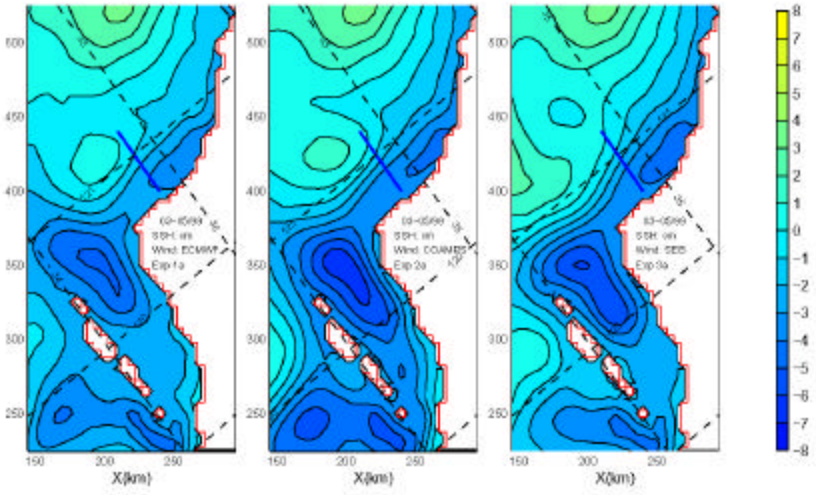


Fig. 5b

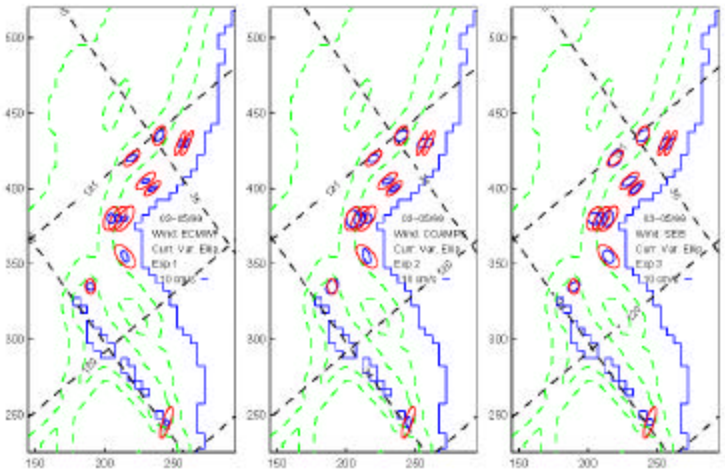

Fig. 6a

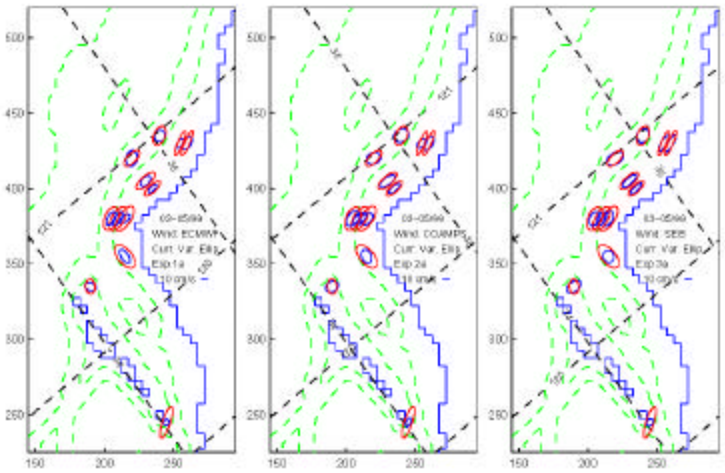

Fig. 6b

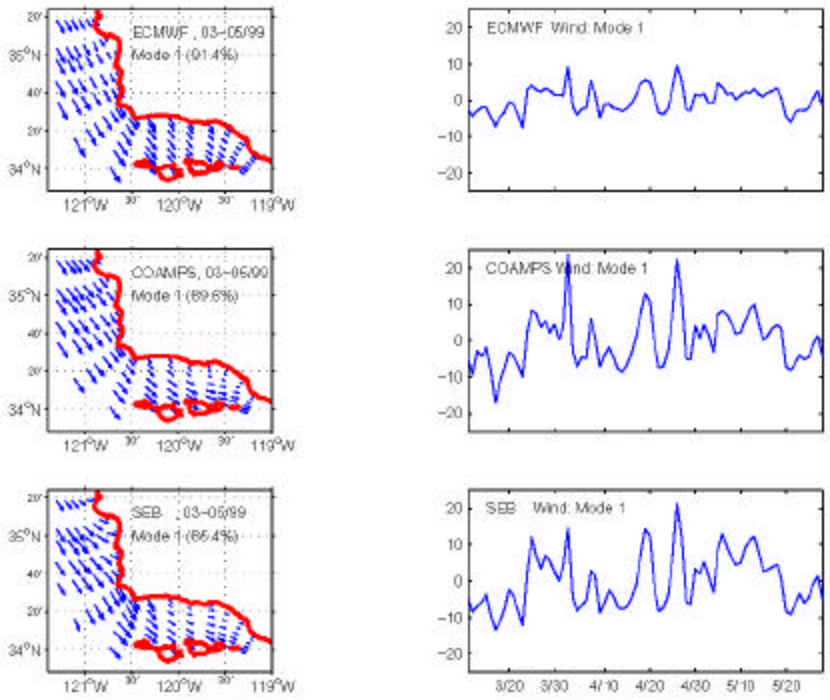
ECMWF , 03-05/99
Mode 1 (91.4%)
COAMPS, 03-05/99
Mode 1 (89.6%)
SEB , 03-05/99
Mode 1 (86.4%)
35°N
34°N
121°W
120°W
119°W
ECMWF Wind: Mode 1
COAMPS Wind: Mode 1
SEB Wind: Mode 1
20
10
0
−10
−20
3/20
3/30
4/10
4/20
4/30
5/10
5/20

Fig. 7

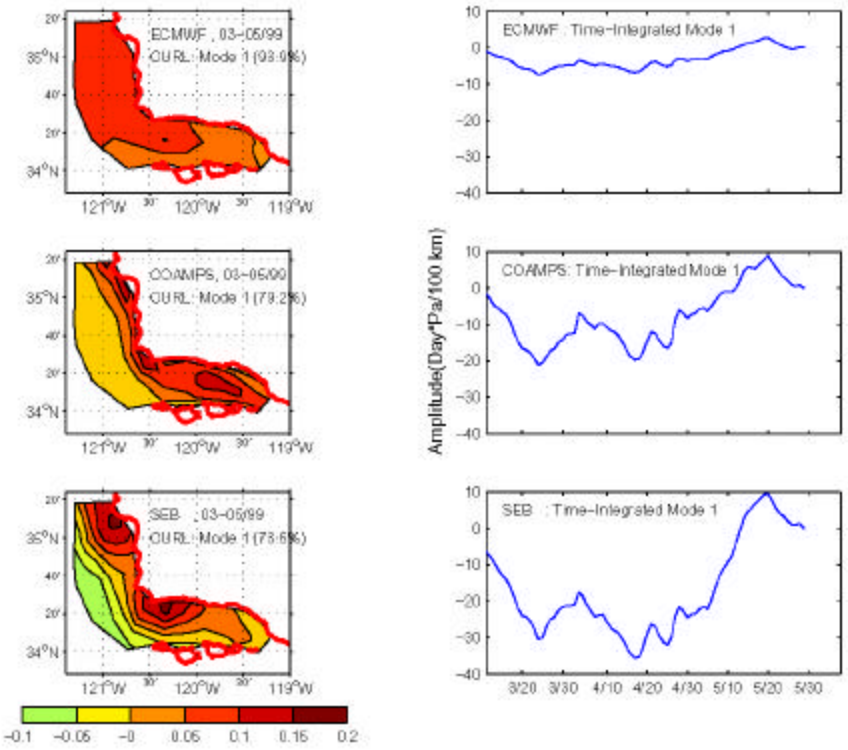
ECMWF , 03-05/99
CURL Mode 1 (93.9%)
COAMPS, 03-05/99
CURL Mode 1 (79.2%)
SEB , 03-05/99
CURL Mode 1 (73.6%)
35°N
34°N
121°W
120°W
119°W
-0.1
-0.05
-0
0.05
0.1
0.15
0.2
ECMWF : Time-Integrated Mode 1
COAMPS: Time-Integrated Mode 1
SEB : Time-Integrated Mode 1
Amplitude(Day*Pa/100 km)
10
0
-10
-20
-30
-40
3/20
3/30
4/10
4/20
4/30
5/10
5/20
5/30

Fig. 8

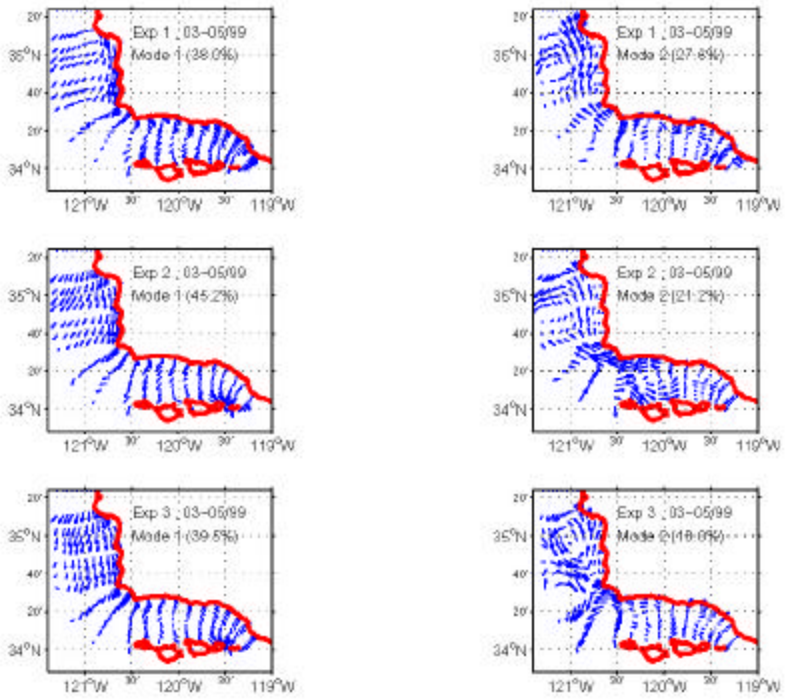
Exp 1 ; 03-05/99
Mode 1 (38.0%)
Exp 1 ; 03-05/99
Mode 2 (27.8%)
Exp 2 ; 03-05/99
Mode 1 (45.2%)
Exp 2 ; 03-05/99
Mode 2 (21.2%)
Exp 3 ; 03-05/99
Mode 1 (39.5%)
Exp 3 ; 03-05/99
Mode 2 (18.6%)
35°N
34°N
121°W
120°W
119°W

Fig. 9a

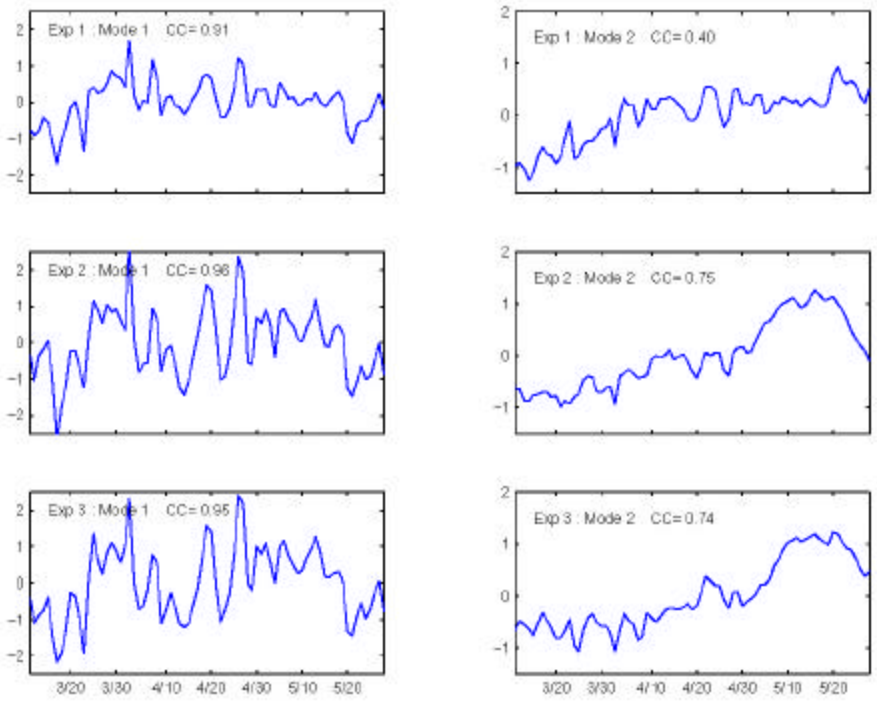
Exp 1 : Mode 1 CC= 0.91
Exp 1 : Mode 2 CC= 0.40
Exp 2 : Mode 1 CC= 0.96
Exp 2 : Mode 2 CC= 0.75
Exp 3 : Mode 1 CC= 0.95
Exp 3 : Mode 2 CC= 0.74
3/20 3/30 4/10 4/20 4/30 5/10 5/20

Fig. 9b

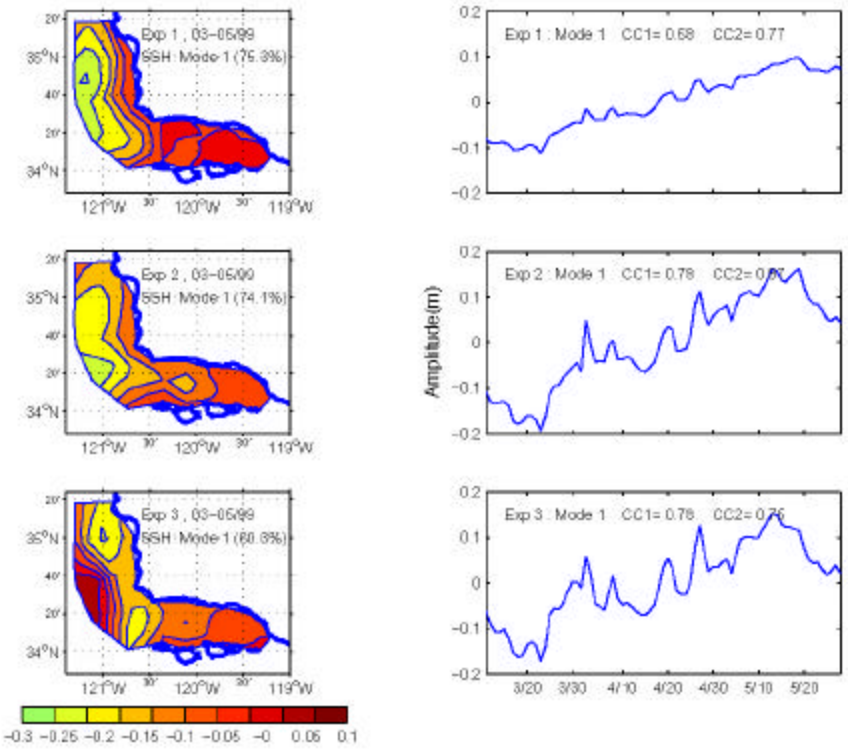
Exp 1 , 03-05/99
SSH Mode 1 (75.3%)
Exp 2 , 03-05/99
SSH Mode 1 (74.1%)
Exp 3 , 03-05/99
SSH Mode 1 (60.8%)
35°N
34°N
121°W
120°W
119°W
-0.3 -0.25 -0.2 -0.15 -0.1 -0.05 -0 0.05 0.1
Exp 1 Mode 1 CC1= 0.68 CC2= 0.77
Exp 2 Mode 1 CC1= 0.78 CC2= 0.87
Exp 3 Mode 1 CC1= 0.78 CC2= 0.76
Amplitude(m)
0.2
0.1
0
-0.1
-0.2
3/20 3/30 4/10 4/20 4/30 5/10 5/20

Fig. 10